



ELSEVIER

Contents lists available at ScienceDirect

## Solid State Communications

journal homepage: [www.elsevier.com/locate/ssc](http://www.elsevier.com/locate/ssc)

# An efficient algorithm for spatially-correlated random fields generation and its applications on the two-phase material

Xin-Wei Tang<sup>a</sup>, Xiao-Bao Yang<sup>b,\*</sup>, Yuan-De Zhou<sup>c</sup><sup>a</sup> Department of Hydraulic and Hydropower Engineering, School of Civil Engineering and Transportation, South China University of Technology, Guangzhou 510640, People's Republic of China<sup>b</sup> Department of Physics, South China University of Technology, Guangzhou 510640, People's Republic of China<sup>c</sup> Department of Hydraulic Engineering, Tsinghua University, Beijing 100086, People's Republic of China

## ARTICLE INFO

## Article history:

Received 12 June 2013

Received in revised form

25 October 2013

Accepted 2 December 2013

Available online 17 December 2013

## Keywords:

A. Composites

D. Elastic properties

E. Simulations

## ABSTRACT

The properties of material strongly depend on the microstructure, and the development of microstructure is closely related to the phase transition with the temperature-dependent spatial correlation. To consider more realistic microstructures, we have proposed an efficient and simple algorithm for generating the spatially-correlated random field, which is obtained by the weighted average of random fields without spatial correlation according to the spatially-correlated length and anisotropy parameter. By using a mesoscale finite element model with the microstructures generated by our algorithm, an application study on the effective elastic behavior of Al<sub>2</sub>O<sub>3</sub>–NiAl composite materials is given. Our numerical results are in agreement with the experimental measurements. The proposed method is general and robust, which can be extended to the multi-phase materials.

© 2013 Elsevier Ltd. All rights reserved.

## 1. Introduction

It has been a challenge to determine the microstructure of a solid, since the final microstructure depends sensitively on the cooling rate and the depth of quench, which is dictated by dynamics and not by energetics alone [1–3]. However, the feature of material, such as dielectric response [2] and magnetic properties [3], strongly depends on its microstructure. For elastically inhomogeneous alloys, the phase diagram of temperature and composition was numerically obtained, in which the effect of elastic inhomogeneity on the phase transition behavior was also discussed [4]. Recently, dense Al<sub>2</sub>O<sub>3</sub>–NiAl composites containing 0–100% NiAl were prepared by sintering, with no chemical reactions and negligible mutual solubility between the two materials [5,6]. The elastic and shear moduli obtained experimentally fall within the Voigt–Reuss bounds and close to the lower bound of the Hashin–Shtrikman (H–S) model, while Poisson's ratio of the composites shows strong dependence on their microstructure characteristics.

In general, the elastic properties of two-phase materials can be obtained through solving the relevant governing equations by various numeric algorithms, such as the traditional finite-difference scheme [7] or the popular finite-element technique

[8,9]. Employing the lattice Boltzmann method [10], the elastic properties of multiphase composites of complex geometries can be determined by numerically solving the stress–strain relationships in heterogeneous materials, where the random microstructures of the multiphase composites were reproduced by the random generation-growth method [11]. Considering the microstructures of materials, the spatial correlation should be taken into account. For example, the fiber networks exhibited long-range power-law spatial correlations of the density and elastic properties, which can be modeled by the stochastic finite element method [12,13]. In concrete and rock material, different tests of varied ingredients or mixture ratios presented different failure patterns and a large scatter in the softening branch of load–displacement response, which may be due to a great variety of the internal correlation length for these artificial materials [14].

The spatial correlation can be easily calculated when the microstructures are determined. However, the microstructures are not unique for a given spatial correlation and the generation of spatially correlated random field is a typically inverse problem. Till now, several iterative methods have been proposed to generate spatially correlated random field, reflecting the realistic microstructures of the multi-phase materials. Besides the Fast Fourier Transform Method by Yaglom [15] and the Turning Bands Method by Matheron [16], Fenton and Vanmarcke [17] presented the Local Average Subdivision Method for the generation of spatially-correlated random field, which was ideally suited to finite element models. In addition, Fang et al. [18] used a multilevel grid strategy,

\* Corresponding author. Tel./fax: +86 2087110427.

E-mail addresses: [scxyang@scut.edu.cn](mailto:scxyang@scut.edu.cn) (X.-B. Yang), [zhouyd@mail.tsinghua.edu.cn](mailto:zhouyd@mail.tsinghua.edu.cn) (Y.-D. Zhou).

which combined the matrix decomposition method and the screening sequential simulation method. However, all these methods require too much complicated operations for practical applications.

Compared to iterative methods, spatially correlated random field can be generated through stochastic optimizing algorithms [19–21], such as the simulated annealing and genetic algorithm. For given spatial correlations, Yeong and Torquato [19] defined the objective function from a squares error between the candidate ones and the objective one, obtaining the required microstructure by searching the least error via the simulated annealing. Similarly, Matouš et al. [20] constructed a fitness function according to the one- and two-point probability functions and minimized the fitness function, using genetic algorithms combined with simulated annealing. In addition, a stochastic Wang tiling-based technique could be applied to reconstruct the microstructures with given spatial statistics, which utilized a finite set of tiles assembled and accurately reproduced long-range orientation orders with high efficiency [21].

In this paper, we propose a simple and practical algorithm to generate the spatially correlated random field, describing the microstructures with the spatial correlated length and the anisotropy parameter. Starting from a series of random number without spatial correlation, we generate new series with the linear composition of origin series, according to the spatial correlation length and the coefficients which are determined by the calculations of spatially-correlated functions. By using mesoscale finite element models with more realistic microstructures generated by our algorithm, the effective elastic behavior of two-phase material is taken as an application study. Our numerical results of Al<sub>2</sub>O<sub>3</sub>–NiAl are in agreement with the experimental measurements. The proposed method is general and robust, which can be extended and applied in the multi-phase materials.

## 2. Methods

The main idea of our algorithm is to generate spatially-correlated random fields from those without spatial correlation, by the weighted average according to the spatially-correlated length and anisotropy parameter. As is known, Ising model has been considered as the typical model to demonstrate the phase evolution, in which the spatial correlation is temperature-dependent following the exponential decay. For simplicity, our method focused on the microstructures with the exponential decaying correlation function. We would investigate the cases with other types of spatial correlations in future work.

For the two-phase material, we firstly consider a one-dimensional random series without spatial correlation  $a_i = \pm 1$ ,  $i = 1, 2, \dots, n$ , where 1 and -1 indicate the two components. Thus, we have

$$\langle a_i a_{i+d} \rangle = \frac{1}{n} \sum_{i=1}^n a_i a_{i+d} = \begin{cases} 1, & d = 0 \\ 0, & d \neq 0 \end{cases} \quad (1)$$

where  $d$  is the distance between  $a_{i+d}$  and  $a_i$ . With the linear composition of  $a_i$  and certain parameters  $c_i$ , we construct a new series  $b_i$  ( $i = 1, 2, \dots, n$ ):

$$b_i = c_0 a_i + \sum_{k=1}^n c_k a_k r^{d(k)} \quad (2)$$

where  $d(k)$  is the effective distance between  $a_i$  and  $a_k$ , and  $r = \exp(-1/L)$ , in which  $L$  denotes the spatial correlation length. Applying the periodical boundary condition, we have  $a_{i+n} = a_i$ . Note that using a linear transformation of the vector of independent random variables is a general technique to produce random

variables with a specified covariance matrix, such as the Cholesky decomposition [22].

For the isotropic material,  $d(k)$  is the absolute value of  $(k-i)$  in the one dimensional case. The correlation of  $b_i$  can be calculated as:

$$\langle b_i b_{i+k} \rangle = \frac{1}{n} \sum_{i=1}^n b_i b_{i+k} = \begin{cases} c_0^2 + O(r), & k = 0 \\ \sum_{j=0}^k (c_j c_{k-j}) r^k + O(r^{k+1}), & k \neq 0 \end{cases} \quad (3)$$

where  $O(r)$  and  $O(r^{k+1})$  are the ignored terms of higher order than  $r$  and  $r^{k+1}$ , respectively. Thus, we should have  $c_0^2 = 1$  and  $\sum_{j=0}^k (c_j c_{k-j}) = 1$ , which confirm

$$\langle b_i b_i \rangle : \langle b_i b_{i+1} \rangle : \langle b_i b_{i+2} \rangle : \dots : \langle b_i b_{i+k} \rangle : \dots = 1 : r : r^2 : \dots : r^k. \quad (4)$$

We set  $c_0$  to be 1 and thus  $c_1$  should be 0.5, since  $c_0 c_1 + c_1 c_0 = 1$ . With  $c_0 = 1$  and  $c_1 = 0.5$ , we can obtain  $c_2$  from  $c_0 c_2 + c_1 c_1 + c_2 c_0 = 1$ . Similarly, the  $c_i$  of larger indices can be obtained. As shown in the inset of Fig. 1(a), the parameters  $c_i$  decrease as the index  $i$  increases. Note that we use the truncation to simplify the calculation of  $c_i$ , which would also induce the discrepancies compared to analytical functions. However, the strict deduction of  $c_i$  is much more complicated.

In the construction of spatial-correlated random field, there are two factors to be determined: the parameter  $c_i$  and the effective distance of  $d$ . Similar to one dimensional case, we construct the new series  $b_{ij}$  for two dimensional cases to maintain the spatial

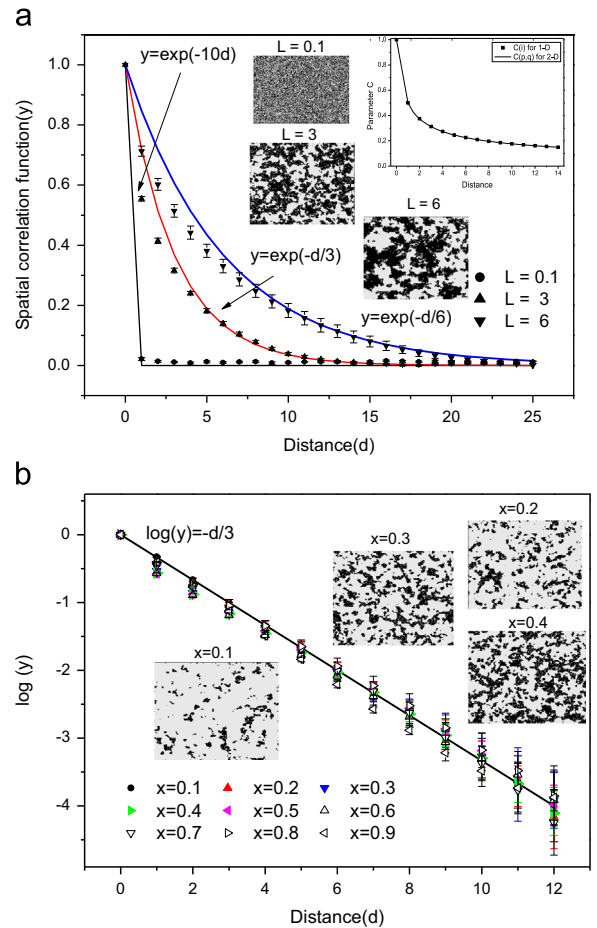


Fig. 1. (Color online) The spatial correlation functions and microstructures obtained by the algorithm for two-dimensional case with various spatial correlation lengths ( $L$ ) and composition ( $x$ ): (a)  $x = 0.5$ ,  $L = 0.1, 3$ , and  $6$ ; (b)  $L = 0.3$ ,  $x = 0.1-0.9$ . The results of analytical calculations are plot in solid lines for comparison, with typical microstructures shown in the inset. The parameters  $c_i$  and  $c_{d(p,q)}$  are shown in the inset of (a).

correlation as

$$b_{i,j} = c_0 a_{i,j} + \sum_{p=1}^n \sum_{q=1}^n c_{d(p,q)} a_{p,q} t^{d(p,q)} \quad (5)$$

where  $c_{d(p,q)}$  are interpolated from the ones that  $d(p,q)$  are integers, as shown in the inset of Fig. 1(a). For the isotropic case,  $d(p,q)$  is  $\sqrt{(p-i)^2 + (q-j)^2}$ . Note that the spatial correlation lengths along different directions are different for the anisotropic case. We introduce another parameter  $s$  ( $s > 1$ ) to define the anisotropy, where  $L_x = L_y/s$ ,  $L_x$  and  $L_y$  are the spatial correlation length along the  $x$  and  $y$  directions. Thus, the effective distance  $d(p,q)$  should be calculated as  $\sqrt{s^2(p-i)^2 + (q-j)^2}$ . To enhance the efficiency, we neglect the contributions when  $d(p,q)$  is more than eight times of spatial correlation length. Using our algorithm, we can obtain a required microstructure of  $500 \times 500$  grid in one or two minutes while hours should be cost when the simulated annealing method is used.

### 3. Results and discussions

As an example, we consider the two-dimensional microstructures of  $A_xB_{1-x}$  alloy generated by our approach on a  $200 \times 200$  grid system, where the composition  $x$  ranges from 0 to 1. Fig. 1(a) shows the spatial correlation functions and microstructures at the composition of 0.5 with different spatial correlation lengths ( $L=0.1, 3$  and  $6$ ). The spatial correlation functions are found to satisfy the analytical ones and the one with  $L=0.1$  can be considered to be with no spatial correlation. As the spatial correlation length increases, the area of domain increases. Note that our algorithm is not rigorous, since the  $b_{i,j}$  series are non-integer values. According to the composition of two phase, we set the threshold value, above/below which corresponds to 1 and  $-1$ , respectively. The spatial correlation functions were calculated using the variables after the transformation with the threshold value. For example, we set the mean value as the threshold one at  $x=0.5$ . Similarly, we obtain the alloy microstructures with the composition  $x \neq 0.5$ , where the initial  $a_{i,j}$  series with various compositions are tested to make the spatial correlation functions match the analytical ones. Due to the truncation deduction of  $c_i$  and the transformation with the threshold value, there are deviations compared to the expected spatial correlation functions. As shown in Fig. 1(b), we used a logarithmic plot of the correlation function for the alloy with  $x=0.1-0.9$ , where the microstructures with  $x=0.1-0.4$  are shown for comparison. We found that there was a linear dependence of the logarithmic plot of the correlation function on the distance, which indicated that the correlation function would follow the exponential decay with the distance to satisfy the analytical spatial correlated function.

Fig. 2 shows the spatial correlation functions and microstructures of the anisotropic alloy, with the spatial correlation length of  $L=6$  and the anisotropic parameter of  $s=1, 3$ , and  $6$ . Thus, the spatial correlation length along the  $Y$  direction ( $L_y$ ) is 6 and the ones the  $X$  direction ( $L_x$ ) are 6, 2 and 1 respectively. The spatial correlation functions are in good agreement with the analytical ones. According to the microstructures, it is found that the stripes parallel to the  $X$  direction become narrower as the anisotropic parameter  $s$  increases.

An application study on the elastic properties of  $Al_2O_3$ -NiAl with various content of NiAl is given in this section using the finite element method. A series of analyses considering different spatial correlation lengths and anisotropic parameters have been carried out to investigate their influence on the material properties. According to the micrographs of  $Al_2O_3$ -NiAl [6], the grain size

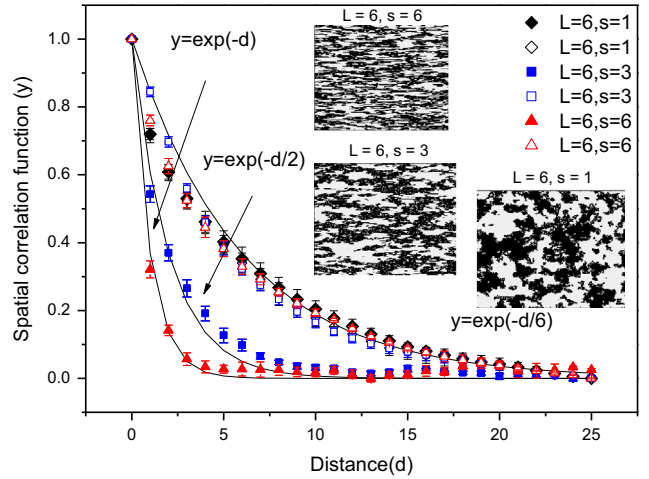


Fig. 2. (Color online) The spatial correlation functions and microstructures obtained by the algorithm for two-dimensional case with various anisotropic parameters. The solid and open markers correspond to the correlation function in the  $x$ -direction and the  $y$ -direction, respectively.

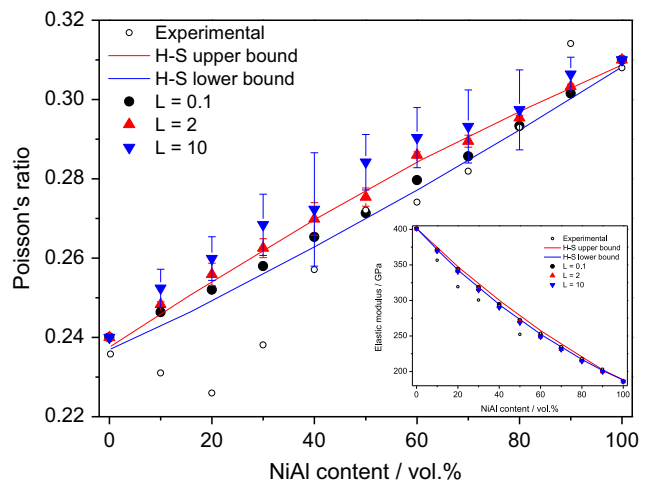
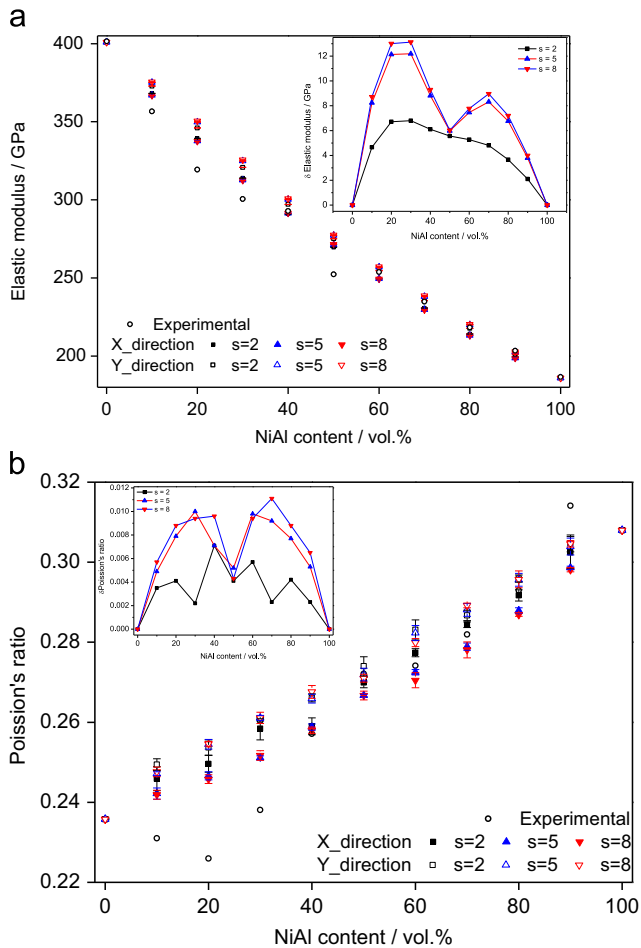


Fig. 3. (Color online) Poisson's ratios of  $Al_2O_3$ -NiAl composites as function of NiAl content with various spatial correlation lengths. Inset is the elastic modulus. The lines are predicted by the H-S model and the data marked with empty circles are obtained from the experimental measurements, as are reported in Ref. [6].

was in the order of  $1 \mu m$  and thus we chose a plane stress square specimen of  $50 \mu m$  in side length, discretizing the specimen into  $0.1 \mu m \times 0.1 \mu m$  finite elements. The elastic modulus and Poisson's ratio of  $Al_2O_3$ /NiAl are 401/186 GPa and 0.24/0.31 respectively, which were determined with the ultrasonic technique in Ref. [6].

For the isotropic cases, three groups of random samples are generated by using a spatial correlation lengths of 0.1, 2 and 10. The first two groups include three numerical samples and the number of samples is increased to 10 for the spatial correlation length of 10. The inset of Fig. 3 shows the variation results of the elastic modulus of  $Al_2O_3$ -NiAl composites as a function of NiAl content. The upper and lower bounds proposed by the H-S model are also shown, which are relatively close to each other and cannot fully contain the test results [6]. Both the displacement loading and force loading conditions have been applied, and the calculation results only show minor difference. It is found that the predicted variations of the elastic modulus strongly depend on the NiAl content, and correspond well with the test results. The variable microstructures induced by different inputs of the spatial correlation length show only minor effects on the prediction



**Fig. 4.** (Color online) The effect of anisotropic parameters on the elastic properties of the  $\text{Al}_2\text{O}_3$ -NiAl composites as a function of NiAl content: (a) elastic modulus and (b) Poisson's ratios. Insets show the differences of elastic modulus and Poisson's ratios along the X and Y directions.

results. A comparison of the simulation and test results of Poisson's ratio is shown in Fig. 3. For the case of  $L=0.1$ , Poisson's ratio lay between the upper and lower bounds of H-S model. However, the calculated variance of Poisson's ratio was found to increase with the spatial correlation length, indicating that Poisson's ratio would be strongly affected by the microstructures of the composite material. Thus, the discrepancies between the experimental results and the H-S bounds might be attributed to spatially-correlated microstructures with larger spatial correlation length.

According to the microstructures obtained in the experiments [6], we selected the spatial correlation length of  $L=3$  and the anisotropic parameter of  $s=5$ . To investigate the anisotropic effect, we generated three groups of random samples with the anisotropic parameter varying amongst 2, 5 and 8, and each group includes three samples. Typical results are given in Fig. 4. We found that both the elastic modulus and Poisson's ratio along the X

and Y directions are different, where the differences increase as the anisotropic parameter increases. The max difference of elastic modulus and Poisson's ratio are 13 GPa and 0.011 respectively, which depends on both the NiAl content and the anisotropic parameter. Note that the increase of anisotropic parameter would not have significant effect on the results when  $s > 8$  for the spatial correlation length of  $L=3$ , since the spatial correlation length along the X direction approach zero gradually with  $L_X = L/s$ .

#### 4. Summary

In summary, we predict the effective elastic behavior of two-phase material, where both the spatially-correlated random fields and mesoscale finite element models have been employed. The proposed algorithm is efficient and simple for generating spatially-correlated random fields, which are obtained by the weighted average of random fields without spatial correlation. Using the  $\text{Al}_2\text{O}_3$ -NiAl composite material as an example, Poisson's ratio was found to be strongly affected by the microstructures as the spatial correlation length and the anisotropic parameter increase. Our results would shed light on the explanation of the experimental results, with discrepancies compared to H-S bounds.

#### Acknowledgments

The authors acknowledge the support by the National Natural Science Foundation of China under Grant nos. 51109083 and 11172321, as well as partial support from Fundamental Research Funds for the Central Universities under Grant nos. 2012ZM0091 and 2013ZZ0082.

#### References

- [1] M. Rao, S. Sengupta, *Phys. Rev. Lett.* 91 (2003) 045502.
- [2] L. Ni, X.M. Chen, X.Q. Liu, R.Z. Hou, *Solid State Commun.* 139 (2006) 45–50.
- [3] Xiao Chun-Tao, Inaba Yuki, Shimatsu Takehito, Muraoka Hiroaki, *Solid State Commun.* 144 (2007) 58–60.
- [4] A. Onuki, A. Furukawa, *Phys. Rev. Lett.* 86 (2001) 452.
- [5] W.H. Tuan, P.Y. Pai, *J. Am. Ceram. Soc.* 82 (1999) 1624.
- [6] C.L. Hsieh, W.H. Tuan, T.T. Wu, *J. Eur. Ceram. Soc.* 24 (2004) 3789.
- [7] J. Poutet, D. Manzoni, F. HageChehade, C.J. Jacquin, M.J. Bouteca, J.F. Thovert, P.M. Adler, *J. Mech. Phys. Solids* 44 (1996) 1587.
- [8] D.P. Mondal, N. Ramakrishnan, S. Das, *Mater. Sci. Eng. A* 433 (2006) 286.
- [9] C.A. Tang, Y.B. Zhang, Z.Z. Liang, T. Xu, L.G. Tham, P.-A. Lindqvist, S.Q. Kou, H.Y. Liu, *Phys. Rev. E* 73 (2006) 056120.
- [10] M. Wang, N. Pan, *J. Comput. Phys.* 228 (2009) 5978.
- [11] M. Wang, J. Wang, N. Pan, S. Chen, *Phys. Rev. E* 75 (2007) 036702.
- [12] H. Hatami-Marbini, R.C. Picu, *Phys. Rev. E* 80 (2009) 046703.
- [13] C. Heussinger, E. Frey, *Phys. Rev. Lett.* 96 (2006) 017802.
- [14] X.W. Tang, Y.D. Zhou, C.H. Zhang, J.J. Shi, *J. Mater. Civ. Eng.* 23 (2011) 402.
- [15] A.M. Yaglom., *An Introduction to the Theory of Stationary Random Functions*, Dover, Mineola, NY, 1962.
- [16] G. Matheron., *Adv. Appl. Probab.* 5 (1973) 439.
- [17] G.A. Fenton, E.H. Vanmarcke, *ASCE J. Eng. Mech.* 116 (1990) 1733.
- [18] J. Fang, L. Tacher, *Commun. Numer. Methods Eng.* 19 (2003) 801.
- [19] C.L. Y. Yeong, S. Torquato, *Phys. Rev. E* 57 (1998) 495.
- [20] H. Lee, M. Brandyberry, A. Tudor, K. Matouš, *Phys. Rev. E* 80 (2009) 061301.
- [21] J. Novak, A. Kucerova, J. Zeman, *Phys. Rev. E* 86 (2012) 040104.
- [22] J.C. Pinheiro, D.M. Bates, *Stat. Comput.* 6 (1996) 289.